RESEARCH PAPER

PCCP
www.rsc.org/pccp

Experimental studies of the photophysics of gas-phase fluorescent protein chromophores

L. H. Andersen,*[a] H. Bluhme,[a] S. Boyé,†[a] T. J. D. Jørgensen,[b] H. Krogh,[a] I. B. Nielsen,[a] S. Brøndsted Nielsen[a] and A. Svendsen[a]

[a] *Department of Physics and Astronomy, Ny Munkegade, University of Aarhus, DK-8000, Aarhus C, Denmark. E-mail: lha@phys.au.dk*

[b] *Department of Biochemistry and Molecular Biology, University of Southern Denmark, DK-5230, Odense M, Denmark*

Received 4th December 2003, Accepted 18th February 2004
First published as an Advance Article on the web 27th April 2004

To better understand the photophysics of photoactive proteins, the absorption bands of several gas-phase biomolecules have been studied recently at the electrostatic heavy-ion storage ring ELISA by a photofragmentation technique. In the present paper we discuss the involved photophysics and photochemistry for protonated and deprotonated model chromophores of the Green Fluorescent Protein (GFP) and the Red Fluorescent Protein (RFP). We show specifically that the delayed dissociation after photoabsorption can be understood in terms of a thermally activated process of the Arrhenius type. The rate of dissociation as a function of time after laser excitation is modeled in a calculation which is based on calculated heat capacities of the chromophores. Absorption of only one photon is enough to dissociate the deprotonated GFP chromophore on a time scale of milliseconds whereas absorption of two to three photons occurs for other chromophore ions. The difference is attributed to different activation energies, pre-exponential factors and locations of the absorption bands. We obtain activation energies for the dissociation that are of the order of 1–3 eV. Collision-induced dissociation experiments were performed to help identifying the fragmentation channels. Loss of methyl is found to be the dominant fragmentation channel for the deprotonated GFP chromophore and is also likely to be important for the protonated GFP chromophore at high temperatures. Other channels are open for the RFP chromophores. For the deprotonated RFP chromophore there is evidence that dissociation occurs through a non-trivial dissociation with substantial rearrangement.

1 Introduction

Chromophores are found in many proteins where they serve as signal mediators in the sense that light absorption by the chromophore has clear detectable consequences. They typically have absorption bands in the visible or near-visible part of the spectrum. In visual pigments, absorption of light triggers fast isomerization of the chromophore[1] producing an active signaling state which eventually generates a visual nerve impulse.[2] Other proteins emit light as a consequence of the primary excitation of the chromophore. Such light-emitting proteins like the Green Fluorescent Protein (GFP) from the jellyfish *Aequorea victoria*[3–6] have immense practical applications in biology for continuously monitoring gene expression and developments in living cells.[3–6] Many GFP mutants have a high fluorescence quantum yield whereas others only have poor quantum yields.[7] The interaction between the chromophore and the protein environment clearly must play a crucial role for the preferred response, for example isomerization *versus* fluorescence. In the case of GFP, fluorescence appears rather robust for the folded protein with a fluorescence-quantum yield of 0.8, but is basically absent when the protein is unfolded.[8] In solution, the chromophore has a fluorescence-quantum yield of only 10^{-3}.[9] Some chromophores like cyanine dyes bind easily to single and double-stranded DNA and are highly fluorescent when bound to DNA while non-fluorescent when free in solution. These proteins are used in many applications involving various DNA-based biological activity.[10] Despite the many applications, important aspects of the photophysics of these chromophores interacting with DNA are still incompletely understood. In the present work we address the basic problem of photo response of chromophores at the most fundamental level, *i.e.*, in the completely isolated form—the gas phase.

In a series of recent experiments we studied gas-phase absorption spectroscopy of model chromophore ions (protonated/deprotonated) of proteins like GFP,[11,12] the GFP mutant called W7,[13] and the red fluorescent protein DsRed.[14,15] The basic idea in these studies was to use the electronic excitation energy (*i.e.*, the absorption wavelength) as a means of monitoring perturbations on the electronic structure of the chromophores in different media like protein cavities and liquids. Thus, using the gas-phase (or vacuum) absorption spectrum as a reference for the zero perturbation case one may get a measure of the perturbations in other media by comparing the absorption profiles. In this way we presented evidence that the unique shape of the GFP protein provides a very efficient protection and isolation of the heart of the protein: its chromophore.

Our previous experimental studies[11–15] were based on a technique where chromophores in the gas phase experienced single or multiple absorptions of photons at a given laser wavelength. As a consequence of the absorption, the chromophores were heated to a degree where they dissociated by thermal activation. The aim of this communication is to discuss the nature of the photo-physical/chemical processes and elucidate the involved molecular dynamics.

† Present address: Laboratoire de Photophysique Moléculaire, CNRS-UPR 3361, Bâtiment 210, Universitéde Paris-Sud, 91405 ORSAY Cédex, France.

DOI: 10.1039/b315763f

2 Experimental

2.1 Storage ring experiment

The experiment was performed at the electrostatic ion-storage ring in Aarhus, ELISA[16] (see Fig. 1). In the storage ring, molecular ions may be stored for several seconds and interactions with for example laser light or electrons may be studied. The chromophore ions were formed by electrospraying a chromophore sample dissolved in an ammoniated water/methanol (1 : 1) solution (pH ~ 11) to obtain the deprotonated form, or in an acetic acid/water/methanol solution (pH ~ 3) to obtain the protonated form of the chromophores. Just after the ion source, a cylindrical ion trap accumulated ions for 0.1 s before they were accelerated as an ion bunch to a kinetic energy of 22 keV. The ions were charge and mass-selected by a magnet and injected into the storage ring. We estimate that a mass-selected ion bunch typically contained about 10^3 to 10^4 ions. In the ring the $1/e$ lifetime was typically 5–10 s limited by collisions with the background gas (pressure *ca.* 10^{-11} mbar). Many technical details concerning the experimental equipment have been given by Andersen *et al.*[17]

After a preselected time of storage, typically 5–50 ms corresponding to about 10^2–10^3 revolutions in the ring, the ions were irradiated by a laser pulse in the straight section opposite the place of injection (see Fig. 1). Storage before irradiation ensured that ions collisionally excited during production and injection had at least partially decayed.[18] We used tunable, visible laser light provided by an optical power parametric oscillator laser (ScanMate OPPO from Lambda Physik) pumped by the third harmonic of a Nd : YAG laser (Infinity-Coherent, 355 nm, 3-ns pulse). Frequency-doubled light from a dye laser (Lambda Physik), pumped by the second harmonic of the Nd : YAG laser, was used for wavelengths shorter than 430 nm. Tuning the laser wavelength to an absorption band resulted in electron detachment and/or bond dissociation and hence production of neutrals. We used a 10 Hz repetition rate and counts of neutrals were normally accumulated over one thousand injections where each injection and storage was associated with only one laser pulse. Neutrals formed in the straight section opposite the laser-interaction region were counted by a particle detector. Because of the low fluorescence quantum yield, the low background rate of neutrals, and the applied single-particle detection scheme, the technique allows us to monitor weak absorption rates. As described below, chromophores in the stored ion bunch absorb photons from a *single* laser pulse. They obtain a high temperature and decay by fragmentation almost exponentially in time. An account for deviations from the exponential decay will be given below.

2.2 Chromophore material

In the present work we used a model chromophore of the Green Fluorescent Protein (GFP)[11,12,19,20] and two model chromophores of the Red Fluorescent Protein, DsRed, (RFP(1), RFP(2))[14,15] found in the *Discosoma striata* coral.[21] A model chromophore of the W7 mutant of GFP (W7) was discussed in some detail recently[13] and will not, for the sake of clearness, be included here. The neutral forms of the chromophores are shown in Fig. 2. The GFP and W7 model chromophores were kindly provided by Steen Uttrup Pedersen, Department of Chemistry, University of Aarhus, and the RFP chromophore material was kindly provided by Peter Tonge and collaborators at the Department of Chemistry, State University of New York at Stony Brook. The GFP and RFP model chromophores share much of the same structure, which originates from the tyrosine amino acid (position 66 in GFP and position 67 in DsRed). In the W7 mutant, tyrosine is substituted by tryptophan at position 66. The two model chromophores of the RFP deviate from those of the GFP in the way that the chromophore called RFP(1) has an additional ethylenic group connected to the imidazolinone ring and RFP(2) has a butadiene group connected at the same position. This extends the conjugation of the chromophore and causes the absorption to be red-shifted relative to that of the GFP chromophore[14] (see Fig. 3).

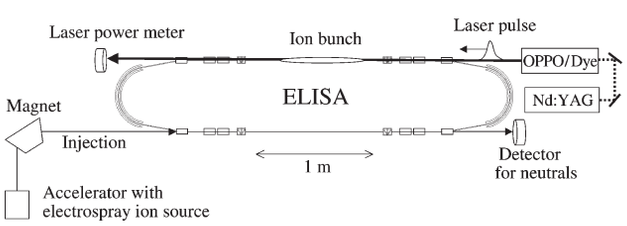

Fig. 1 The electrostatic ion storage ring ELISA equipped with an electrospray-ion source, a pulsed laser and detector for neutral products.

2.3 Low-energy collision-induced dissociation

To help identify the dissociation channels, low-energy collision-induced dissociation (CID) spectra were acquired on an Esquire-LC quadrupole ion trap mass spectrometer (Bruker Daltonik, Bremen, Germany) equipped with a nanoflow electrospray ion source. Samples were electrosprayed from borosilicate capillaries coated with Au/Pd (Proxeon, Odense, Denmark). CID spectra were obtained in enhanced resolution mode with a scan speed of 2000 amu s^{-1}. The accumulation time was automatically determined by the ion charge control feature (ICC, set to 5×10^4) which prevents overloading of the trap. For CID experiments, precursor ions were isolated (isolation m/z window width = 2) and collisionally activated for 40 ms with a fragmentation amplitude of 0.4 to 0.6 V.

3 Calculational details

Calculations were done with the Gaussian98 program package.[22] Geometries were optimized and frequencies calculated at the semiempirical PM3 level of theory. All vibrational frequencies are positive, and the located stationary points are

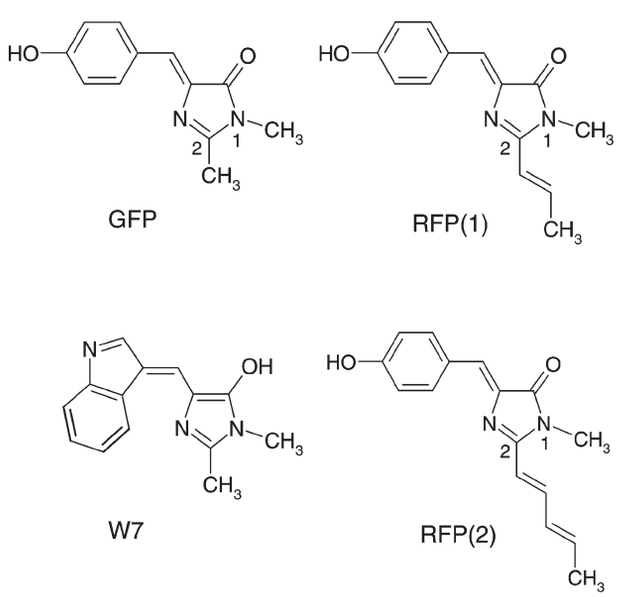

Fig. 2 Chromophores used in the present work (GFP and RFP) as well as the W7 mutant studied earlier.[13] Only neutral forms of the chromophores are shown. For more discussions of the protonation stages of the chromophores see our previous works.[11–15] Note the extended conjugation of the chromophores RFP(1) and RFP(2) compared to the GFP-model chromophore.

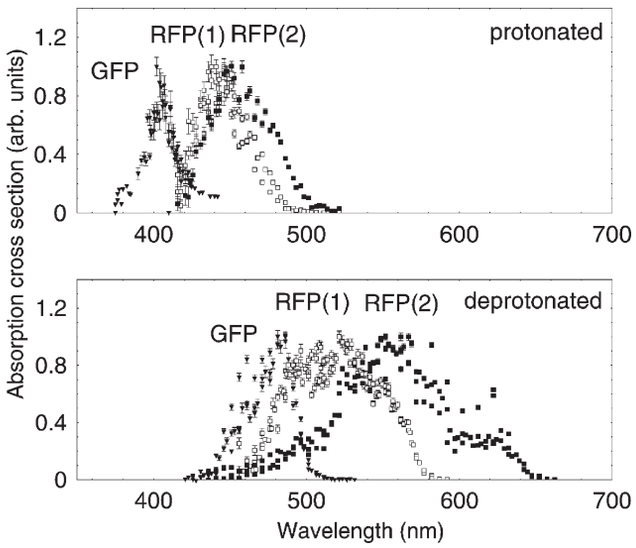

Fig. 3 Absorption cross sections obtained at ELISA for protonated and deprotonated forms of the GFP model chromophore and the two RFP model chromophores studied in the present work.

local minima on the potential energy surfaces. Single-point energies were calculated at the B3LYP/6-311++G(2d,p) level of theory.

4 Results and discussion

4.1 Experimental decay spectra

A series of measurements with the deprotonated GFP chromophore (labeled GFP^-) is shown in Fig. 4. The absorption maximum of this chromophore was found to be at 479 nm.[11] The laser was fired 74.8 ms after the injection and caused an immense production of neutral fragments, the yield of which decayed with time in a way which was not exponential. The production of neutral fragments was basically completed after a few milliseconds. It is seen that the decay is fastest for absorption of photons at the shortest wavelength corresponding to the highest energy and hence highest temperature of the chromophore after absorption. The curves shown in the figure are from a calculation which will be discussed later.

As seen in Fig. 5, the situation is quite different when considering the protonated GFP chromophore (labelled GFP^+). Here the decay is extremely fast at the absorption maximum, which was found to be at 406 nm.[12] However, at shorter wavelengths the decay becomes slower. At 266 nm the decay is about 1000 times slower than at 395 nm! It is also noticed that at, for example, 380 nm there are two decay components in the data—one which corresponds to the extremely short one at the absorption maximum and one with a long decay time which is of the same order as the long component of the 266-nm spectrum.

Decay spectra of the chromophores of the red fluorescent protein are shown in Fig. 6. The displayed data were recorded near the absorption maxima of the chromophores. The two protonated forms, $RFP(1)^+$ and $RFP(2)^+$, exhibit a decay with one main time component, whereas deprotonated chromophores, $RFP(1)^-$ and $RFP(2)^-$, show a fast as well as a slow component. Similar decay curves were recorded over the whole absorption region. Note at this point that the decay for these chromophores is almost exponential in time, unlike the case of the GFP chromophores. An interpretation of the data will follow later in the paper.

4.2 Collision-induced dissociation

Loss of methyl is by far the dominant fragmentation channel in CID of the GFP^-, as seen in Fig. 7. According to B3LYP/6-311++G(2d,p)//PM3 calculations the methyl originates from the nitrogen (position 1) and not from the carbon

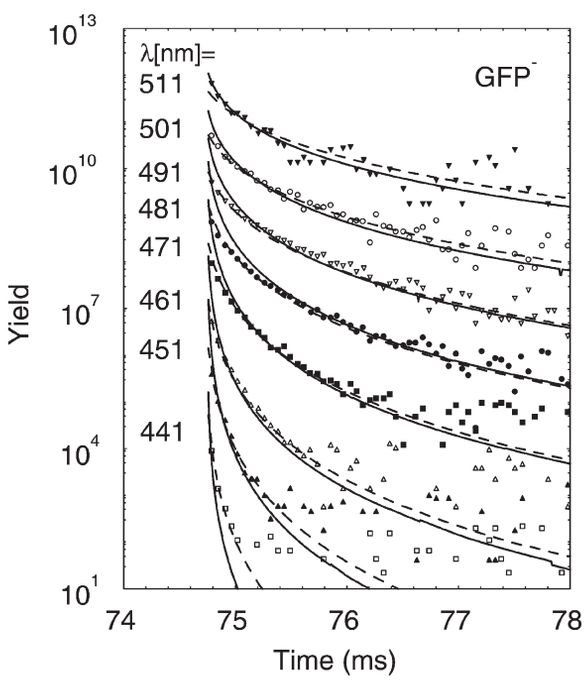

Fig. 4 Yield of neutrals detected after injection of deprotonated GFP chromophores into ELISA. The ions were irradiated after 74.8 ms of storage (the wavelength in nm is indicated at each curve). The data have been multiplied by different factors for the purpose of better display. The curves shown for each wavelength are from calculations with $A = 10^{17}$ s^{-1} and $E_a = 2.06$ eV (solid curves) and $A = 1.6 \times 10^{15}$ s^{-1} and $E_a = 1.82$ eV (dashed curves).

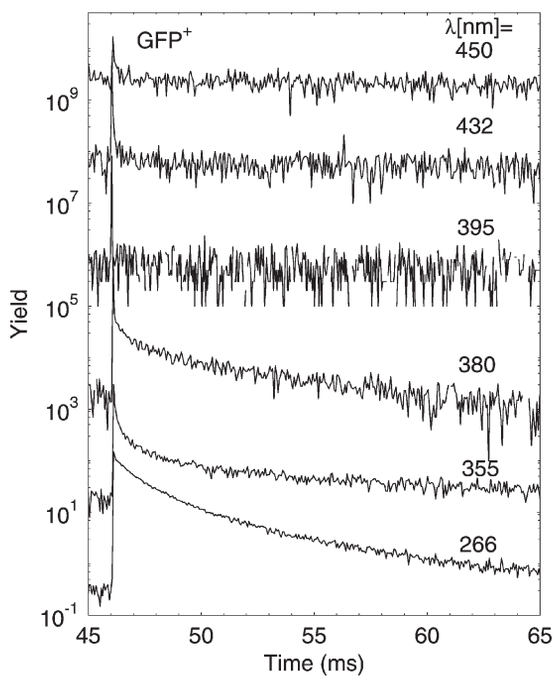

Fig. 5 Yield of neutrals detected after injection of protonated GFP chromophores into ELISA. The ions were irradiated after 46 ms with photons at the wavelength indicated on the figure. The absorption maximum for this chromophore is at 406 nm. The data have been multiplied by different factors for the purpose of better display. Light of 355 nm and 266 nm was obtained as the third and fourth harmonics, respectively, of the Nd : YAG laser.

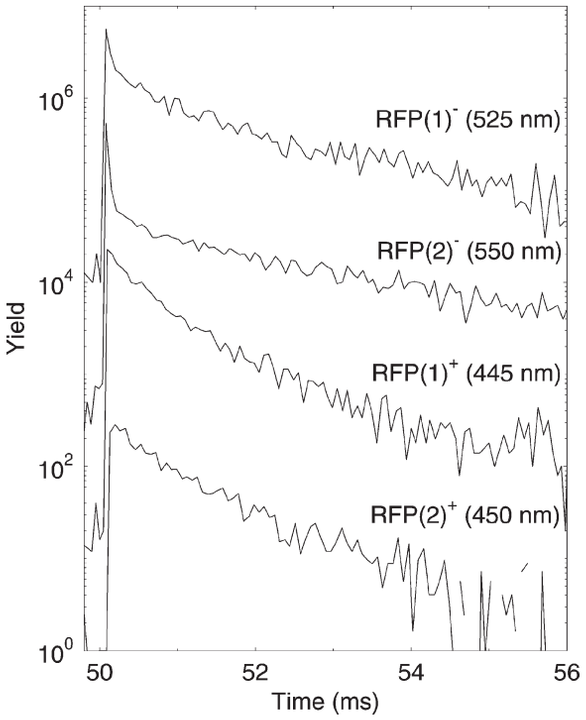

Fig. 6 Yield of neutrals detected after injection of protonated and deprotonated DsRed model chromophores into ELISA (from top to bottom: $RFP(1)^-$, $RFP(2)^-$, $RFP(1)^+$, $RFP(2)^+$). The data were recorded close to the absorption maximum of each chromophore. The ions were irradiated 50 ms after the injection. The data have been multiplied by different factors for the purpose of better display.

(position 2) of the ring since the reaction energy is 2.1 eV and 4.1 eV for the two channels, respectively (see Tables 1 and 2 and the numbering on Fig. 2). Thus, the lower reaction in Scheme 1 is associated with the smallest reaction energy.

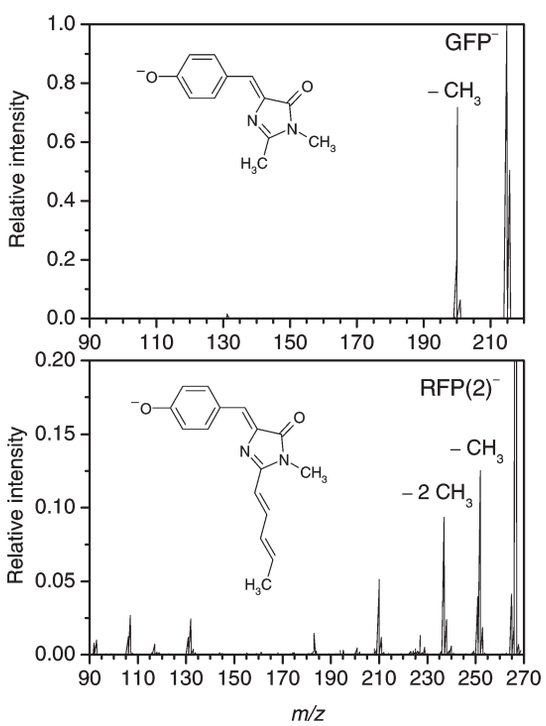

Fig. 7 Collision-induced dissociation spectra of the deprotonated GFP chromophore ($m/z = 215$; upper graph) and the deprotonated RFP(2) chromophore ($m/z = 267$; lower graph). m is the fragment mass in amu and z is the charge of the fragment in units of the electron charge. The peaks are normalized relative to the parent ion.

Table 1 Dissociation energies (eV) of the chromophore ions for the release of the methyl group from the nitrogen atom at position 1 (see numbering in Fig. 2). Calculations at the B3LYP/6-311++G(2d,p)//PM3 level of theory

Chromophore	GFP	RFP(1)	RFP(2)
Anions	2.1	2.0	2.2
Cations	3.4	3.4	3.4

Table 2 Dissociation energies (eV) of the chromophore ions for the release of groups (CH_3 for GFP, $CH{=}CHCH_3$ for RFP(1), and $CH{=}CHCH{=}CHCH_3$ for RFP(3)) from the carbon atom at position 2 (see numbering in Fig. 2). Calculations at the B3LYP/6-311++G(2d,p)//PM3 level of theory

Chromophore	GFP	RFP(1)	RFP(2)
Anions	4.1	4.7	4.8
Cations	4.7	5.5	5.7

The calculated reaction energy for loss of methyl from the nitrogen at position 1 in the case of RFP(1) and RFP(2) anions is similar to that of GFP^- and this channel should still be open. Indeed, the CID spectrum reveals that CH_3 loss from the RFP(2) anion is an important reaction channel but several other fragment ions are also present in the spectrum (see Fig. 7).

The fragmentation spectrum of GFP^+ is not as simple as the spectrum of GFP^-. As seen in Fig. 8 there are two major peaks at $m/z = 186$ and $m/z = 160$ corresponding to loss of neutral fragments of mass 31 amu and 57 amu, respectively. Selection of the $m/z = 186$ fragment ion for CID results in an ion at $m/z = 158$ (see Fig. 8, lower part). Hence, the ion at $m/z = 160$ (Fig. 8 upper part) is not produced by subsequent dissociation of the $m/z = 186$ ion. We tentatively ascribe the $m/z = 186$ ion to be a result of loss of neutral CH_3NH_2 to produce an ion that easily loses CO to give the observed $m/z = 158$ ion. In contrast, the $m/z = 160$ ion is assigned to be due to loss of $CH_3{-}N{=}C(CH_3)H$. Both channels involve two bond dissociations of the five-membered ring. The chromophore possesses two basic nitrogens that can both be protonated (see Fig. 2). It is therefore possible that two isomers are present in the ion beam that may yield either the $m/z = 186$ fragment ion (isomer where the methylated nitrogen is protonated) or the $m/z = 160$ fragment ion (isomer where the other nitrogen is protonated).

4.3 The photocycle

The energy increase per photon absorption is *ca.* 2.5 eV for a chromophore with an absorption band at 500 nm. With about 100 normal modes the average energy per mode is *ca.* 200 cm^{-1}

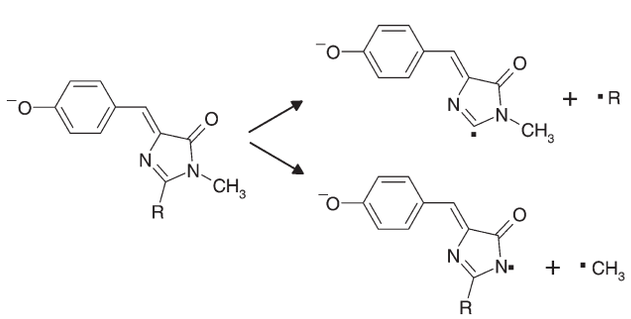

Scheme 1

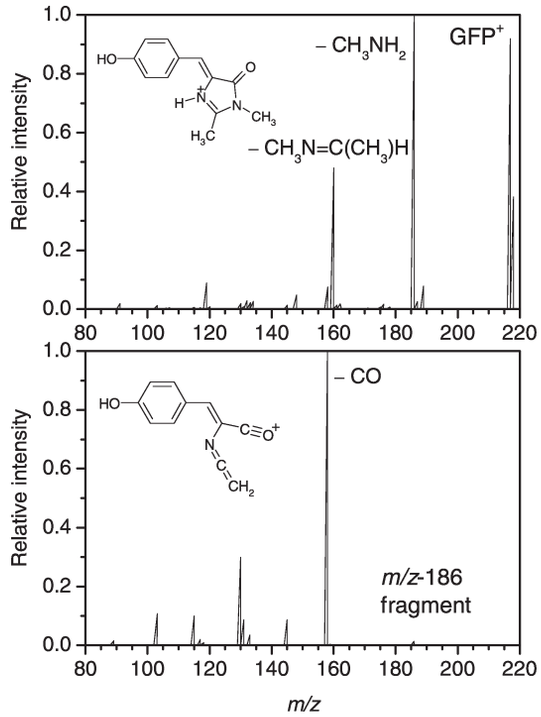

Fig. 8 Collision-induced dissociation spectra of the protonated GFP chromophore ($m/z = 217$; upper graph) and of the $m/z = 186$ fragment which shows a dominating loss of mass 28—detection of $m/z = 158$ (lower graph).

and each oscillator is hence not highly excited.[23] We assume here that we start with a molecule of zero vibrational excitation occupying the electronic ground state S_0 (see Fig. 9). The initial photon absorption (1) brings the molecule into the first excited state of the same spin multiplicity S_1. The absorption profile for this transition is quite broad reflecting the fact that there may be a reasonable Franck–Condon overlap to several vibrationally excited levels of S_1.

Once in the electronically excited state (S_1) several processes are competing. There may be internal conversion (IC) of electronic energy into vibrational energy by the $S_1 \rightarrow S_0$ transition (2) or intersystem crossing $S_1 \rightarrow T_1$ (4a). Different effects play a role when the rates for internal conversion and intersystem crossing are considered. The oscillatory behavior of the

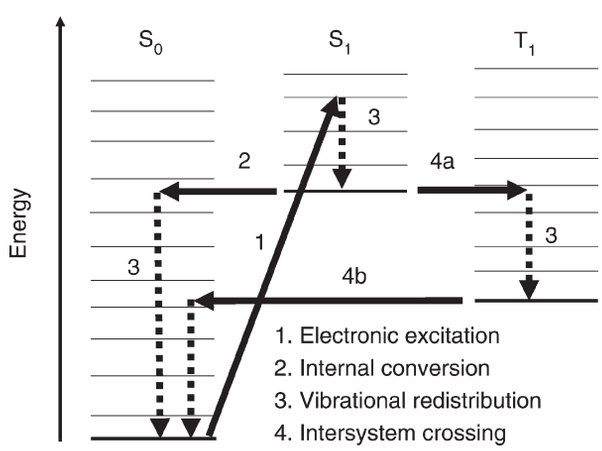

Fig. 9 Schematic representation of the photoresponse of the chromophore. Vibrational energy levels for some vibrational modes are sketched. The vibrational redistribution (3) is concerned with energy transfer into other normal modes (emission of infrared radiation is slow (ms) and hence neglected). We ignore the role of higher excited electronic states S_n and T_n ($n \geq 2$) since $S_n \rightarrow S_1$ and $T_n \rightarrow T_1$ internal conversions are normally very fast.

vibrational wave functions of, in particular, the highly excited states may yield a small Franck–Condon overlap which tends to suppress, in particular, the $S_1 \rightarrow S_0$ IC-transition. On the other hand, there may be a preference for transitions involving highly excited vibrationally states due to the enhanced density of states. The $S_1 \rightarrow T_1$ and $T_1 \rightarrow S_0$ intersystem crossings are normally limited by the size of the spin–orbit coupling.

Intramolecular vibrational redistribution (IVR)(3), where excess quanta of certain vibrational modes redistribute to other modes, will normally take place before internal conversion $S_1 \rightarrow S_0$ or intersystem crossing $S_1 \rightarrow T_1$. In the case of the retinal chromophore there seems to be a very fast ($\leq$100 fs) stretch deformation of the chromophore, which brings the chromophore out of the Franck–Condon region, followed by a slower 'twisting' motion, which takes the system down the S_1 surface until an efficient conversion to the ground state takes place most likely by a conical intersection.[24,25] The group of Meech has specifically shown that in solutions, the GFP-model chromophore decays within 0.5 ps.[19,26] This fast internal conversion may naturally be coupled to the solvent, yet IC may also proceed very fast in isolated molecules when the excited-state surface S_1 at a certain geometry gets very close to the S_0 ground-state surface or even touches it at a conical intersection.[27] The electronic structure of the chromophores used in the present work has been treated theoretically by several groups.[28–32] Although it may be debated along which route the excited state relaxation takes place and to what degree there may be energy degeneracy between S_0 and S_1, it seems reasonable to assume that at room temperature, where small barriers may be passed, the fluorescence yield is very low as a consequence of fast internal conversion.

Photochemistry can take place from the excited singlet or triplet-state manifold. The laser excitation may yield *cis*-conformers in the polyenic chain or N-methyl rearrangements.[33] When the system is back into the electronic ground state S_0 by internal conversion (2) or by a second intersystem crossing $T_1 \rightarrow S_0$ (4b), IVR occurs and the excess energy gets statistically distributed over the $3N-6$ degrees of freedom—again individual oscillators, on average, do not have much energy and most of the time they thus occupy the lowest vibrational levels.

IVR is expected to happen on a short timescale (comparable to the vibrational oscillator times), *i.e.* picoseconds or faster. The time for internal conversion is naturally very dependent on specific molecular structures, overlap of nuclear wave functions, the electronic coupling between the states, and the energy gap. If the structure is not too rigid, the rate $k_{IC(S_1-S_0)}$ may be of the order of 10^5–10^8 s^{-1}.[34] If the energy surfaces S_1 and S_0 undergo a crossing/conical intersection at an accessible nuclear geometry, the rate of the internal conversion may naturally be faster, *i.e.* subpicoseconds. The intersystem crossing (ISC) rate $k_{ISC(S_1-T_1)}$ depends specifically on the spin–orbit coupling, and for the chromophores considered here without atoms heavier than oxygen, $k_{ISC(S_1-T_1)}$ is typically of the order of 10^6–10^9 s^{-1}, although much higher rates are found for some molecules.[34] Presumably, the other intersystem crossing $T_1 \rightarrow S_0$ has a rate $k_{ISC(T_1-S_0)}$ of 10^3 s^{-1} at the most, corresponding to a triplet-state lifetime in the ms regime. If higher states S_n and T_n are involved, for example when excitation is performed by 266 nm, there is normally a very rapid (ps) conversion to the lowest states: $S_n \rightarrow S_1$ and $T_n \rightarrow T_1$ and, as a consequence, we neglect these states in the present discussion.[34]

The cycle involving the triplet state: (1) → (3) → (4a) → (3) → (4b) → (3) is limited by the slow rate $k_{ISC(T_1-S_0)}$ and is thus completed on the ms time scale. Some of our data (see Figs. 4–6) exhibit decays which are on this time scale, and simulations of level populations where a laser-pulse initially excites a chromophore to the S_1 excited state were therefore performed. The excited S_1 state may decay (after fast IVR) to the triplet state T_1 with a rate $k_{ISC(S_1-T_1)}$, or to the singlet

ground state S_0 with a rate $k_{IC(S_1-S_0)}$. The triplet state may after (fast) IVR couple to the electronic ground state S_0 with a rate $k_{ISC(T_1-S_0)}$. After having returned to the electronic ground state the chromophore is assumed to fragment (due to the increased temperature) with a rate $k_{fragment}$. The result of such a simulation is shown in Fig. 10. In the simulation rather low rates of $k_{IC(S_1-S_0)}$ and $k_{ISC(S_1-T_1)}$ were used for the purpose of illustration. The ISC rate $k_{ISC(T_1-S_0)}$ is relatively low, 10^2 s^{-1}, and the fragmentation rate high, $k_{fragment} = 10^4$ s^{-1}. The two clearly distinguishable components in the yield of fragments as a function of time are seen with slopes corresponding to the two rates $k_{ISC(T_1-S_0)}$ and $k_{fragment}$. However, only one component is resolved in the fragmentation yield with a slope corresponding to the lowest rate $k_{fragment}$ when for example the ISC rate $k_{ISC(T_1-S_0)}$ is higher, 10^3 s^{-1}, and the fragmentation rate lower, $k_{fragment} = 10^2$ s^{-1}. The conclusion is that population trapping in the triplet state may sometimes be visible, but not always.

The fast cycle involving only singlet states lasts normally shorter than the laser-pulse duration (ns) and it is possible that additional absorption cycles may take place while the light pulse is still on with the result that the molecule gains the energy $\Delta E = nh\nu$, n being the number of photons absorbed. If chromophores are trapped in a slowly decaying triplet state (T_1), they may also absorb additional photons from the laser pulse due to $T_1 \rightarrow T_n$ transitions, but the cross section for such excitations is most likely small at the wavelength of the $S_0 \rightarrow S_1$ excitation wavelength. When sufficient energy is gained, the molecule eventually decays by particle emission since radiative cooling is normally slow (*ca.* ms).

A high rate for internal conversion results in a small fluorescence yield for the isolated gas-phase chromophore. One may speculate about the reason for a high fluorescence quantum yield in the fluorescent proteins. It is possible that it is high because the chromophore is constrained inside the protein and is hence not free to isomerize;[9,28,35,36] however, this is still being investigated and the role on conical intersections played by external perturbations is also being considered.[37]

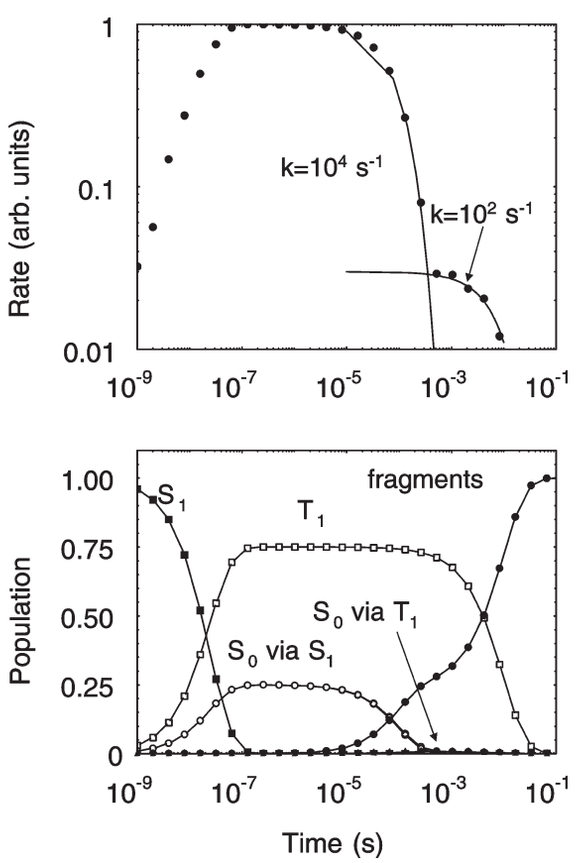

Fig. 10 Simulation of level population (lower figure) with: $k_{IC(S_1-S_0)} = 10^7$ s^{-1}, $k_{ISC(S_1-T_1)} = 3 \times 10^7$ s^{-1}, $k_{ISC(T_1-S_0)} = 10^2$ s^{-1}, and $k_{fragment} = 10^4$ s^{-1}. This results in two visible components in the fragmentation rate with slopes corresponding to $k_{ISC(T_1-S_0)}$ and $k_{fragment}$ (top figure).

4.4 Model calculations

The aim is to generate decay curves (*i.e.*, the yield of neutral fragments as a function of time after laser excitation) for the chromophore ions in the gas phase after absorption of a number of photons (n) from a laser pulse of energy ε and wavelength λ. The following issues will be discussed:

(i) The distribution in the number of absorptions, *i.e.*, how large a fraction of the ions absorbed $n = 1, 2, 3$, *etc.* photons.

(ii) The internal temperature after photon absorption.

(iii) Inclusion of the canonical energy distribution of the molecules prior to excitation and determination of the decay rate after single and multiple photon absorption.

4.4.1 Distribution of absorptions. As discussed above, the non-radiative conversion of electronic energy into vibrational degrees of freedom often happens on a ps time scale, which is short compared to the time duration of the laser pulse (ns). The chromophore may thus absorb more than one photon during the time of exposure to the laser light, the number being limited by the total flux of photons that the chromophore is exposed to and the cross section for single-photon absorption σ. We assume that absorptions happen independently and the distribution of the number of photons will be according to Poisson statistics:

$$P(n) = (\nu)^n/n! \times \exp(-\nu). \quad (4.1)$$

Here, ν is the average number of photons absorbed during the laser pulse, which is given by (cross section times flux):

$$\nu = \sigma \frac{\varepsilon\lambda}{Ahc}, \quad (4.2)$$

where A is the laser-beam area. As argued above, each oscillator is on average not highly excited and it is therefore not expected that differences in Franck–Condon factors play a crucial role. The cross section for absorption is hence assumed to be independent of possible previous absorptions.[38]

The power dependence of the yield of neutral photofragments of the GFP chromophores is shown in Fig. 11. It appears that the anion photodissociates as a result of one-photon absorption at 495 nm and the fragments of the cation at 410 nm are a consequence of two-photon absorption.

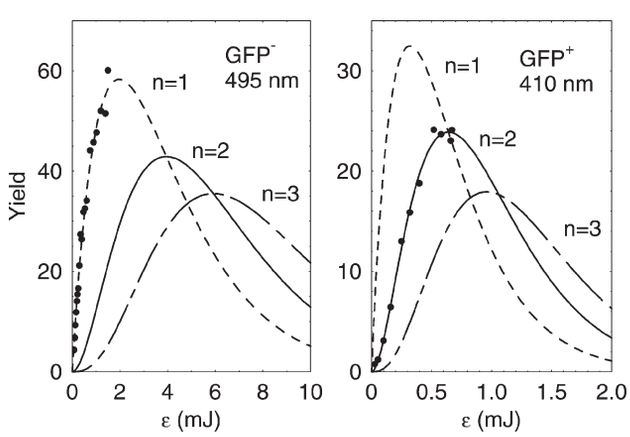

Fig. 11 Yield of neutral fragments from GFP^- and GFP^+ integrated over time as a function of the laser-pulse energy. The curves correspond to $n = 1$, 2, and 3 of the Poisson distribution.

It should be emphasized at this point that it is often exceedingly difficult to establish the correct power-dependence of the neutral yield since all curves over a broad power interval grow almost linearly with power. At the low-power region where the curves corresponding to $n = 1,2,3$ differ in slope, a correct normalization and correction for collisional fragmentation is crucial, but difficult. Moreover, as seen in Fig. 5 for GFP cations at the absorption maximum, the decay is very fast and basically over by the time the ion bunch has moved to the side of ELISA where the detector is located. At the absorption maximum, the decay after one-photon absorption is very slow in the GFP^+ case. Only at the shorter wavelengths below 380 nm (see Fig. 5) does the one-photon component become pronounced with a decay time of several ms. On the other hand, the fast two-photon component disappears at the shorter wavelength because this part of the decay is completed before the ion bunch has moved towards the detector in ELISA.

The yield of neutrals *versus* laser-power for the RFP chromophores showed that the protonated molecules $RFP(1)^+$ and $RFP(2)^+$ fragmented as a result of two-photon absorption. The deprotonated versions, $RFP(1)^-$ and $RFP(2)^-$, exhibit a fast component which is due to three-photon absorption and a long component which is due to two-photon absorption (see Fig. 6).

4.4.2 The internal temperature after absorption. Absorption of n photons increases the internal energy by $\Delta E = nhc/\lambda$, and this raises the temperature of the molecule according to $\Delta T = \Delta E/C$, where C is the microcanonical heat capacity, which asymptotically (*i.e.* at high temperature) is $C = (3N-7)k_B$, k_B being Boltzmanns constant and N the number of atoms in the molecule. Note that C is reduced by k_B, which is due to the fact that the system is not in equilibrium with a heat bath, as is normally the case, and hence we deal with a microcanonical ensemble.[39]

The internal energy at a given temperature is calculated from the normal mode frequencies (ν_i):[40]

$$E = \sum_i [h\nu_i / \exp(h\nu_i/k_B T) - 1], \qquad (4.3)$$

where the sum is over all normal mode frequencies. They were calculated with a semi-empirical method using the PM3 Hamiltonian (Gaussian98[22]). Accordingly, the canonical heat capacity is:

$$C = k_B \sum_i \Big[(h\nu_i/k_B T)^2 \times \exp(-h\nu_i/k_B T) / (1 - \exp(-h\nu_i/k_B T))^2 \Big]. \qquad (4.4)$$

Fig. 12 shows the canonical heat capacity as well as the internal energy as a function of the temperature of the six chromophore molecules used in the present work. The difference between the microcanonical and the canonical heat capacity can to a good approximation be ignored for the present molecules with about 30 atoms. Note that the internal energy at room temperature (E_0) is of the order of 0.3–0.5 eV and that the asymptotic expression for the heat capacity ($C = (3N-6)k_B$) is not valid below 2000 K, which is the region of interest in the present context.

4.4.3 The decay rate. The decay leading to emission of neutral particles is assumed to proceed through a decay channel with activation energy E_a, and the Arrhenius expression for the decay constant is expected to be applicable:

$$k_n = A \times \exp(-E_a/k_B T^*_n), \qquad (4.5)$$

where A is the pre-exponential factor correlated with the mode of decay, and T^*_n is the effective temperature of the molecule

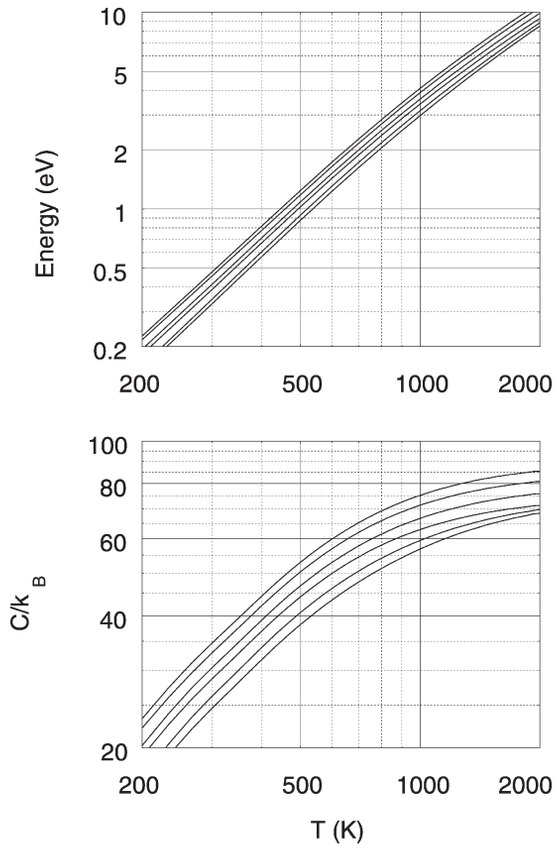

Fig. 12 The calculated internal energy and canonical heat capacity as a function of the temperature of the chromophore ions. The curves from the bottom to the top correspond to: GFP^-, GFP^+, $RFP(1)^-$, $RFP(1)^+$, $RFP(2)^-$, $RFP(2)^+$.

after absorption of n photons. Since the molecule is not in equilibrium with a heat bath which keeps its temperature constant, we operate with an effective temperature T^*_n, which is the temperature corresponding to the mean energy before $(E_0 + E)$ and after $(E_0 + E - E_a)$ the decay:[39]

$$T^*_n = T_n - 1/C_n \times E_a/2, \qquad (4.6)$$

where T_n and C_n is the temperature and heat capacity, respectively, after n-photon absorption. By inspection of Fig. 12 one finds that $C_{n=1}$ is of the order of $50–70 \times k_B$ and for $E_a \sim 2$ eV, the last correction term becomes of the order of 200 K and cannot be neglected. Note also that the effective temperature depends on the activation energy E_a.

It is assumed that the dissociation of the molecule yields some neutral fragments, which may readily be detected in the experiment. Dependent on A and E_a it may take one or several photons to effectively heat up the molecule to cause fragmentation. In the region of absorption (400–600 nm), temperatures of 800–1000 K ($n = 1$) and 1300–1500 K ($n = 2$) are typically reached (see Fig. 12).

The decay in time of an excited chromophore having absorbed n photons is

$$Y_n(t) = k_n \exp(-k_n t) = A \times \exp(-E_a/k_B T^*_n) \times \exp(-A \times \exp(-E_a/k_B T^*_n)t). \qquad (4.7)$$

To get a proper description of the decay, we consider the energy spread (fluctuations) of the initial energy distribution at the appropriate temperature before the photon absorption T_0 (here room temperature). The initial distribution at this temperature is to a good approximation gaussian:[39]

$$G(E) = \frac{1}{\sqrt{2\pi}\sigma_E} \times \exp\left(-E^2/\left(2\sigma_E^2\right)\right), \qquad (4.8)$$

where $\sigma_E = \sqrt{k_B \times C_0}\, T_0$. C_0 is the heat capacity at temperature T_0. The width σ_E is typically 0.1–0.2 eV and can normally not be ignored when only a few photons are absorbed. It is the finite width which is causing a deviation from a perfect exponential decay (see, for example, Figs. 4 and 5). Deviations are most pronounced at low excitation energy ($n = 1$, long wavelength) where σ_E/E is significant. The initial energy spread becomes less important when the activation energy and the pre-exponential factor are low, and the decay will appear almost exponential in this case.

The final expression for the intensity of neutral fragments as a function of time is:

$$I_n(t) = \int dE G(E) k_n(E) \exp(-k_n(E)t), \qquad (4.9)$$

where

$$k_n(E) = A \times \exp(-E_a/k_B(T_n - (1/C_n)E_a/2 + E/C_n)). \qquad (4.10)$$

It is possible to determine both E_a and A with only a single measurement at a given wavelength under certain favorable conditions. However, recording the decay rate at different wavelengths (hence temperatures) provides a better way to determine these parameters simultaneously.

4.5 Fragmentation

In the framework of transition-state theory the pre-exponential factor A of eqn. (4.5) corresponds to the motion along a one-dimensional reaction coordinate, which is not known *a priori*. It may be expressed in the following way:[41]

$$A = \frac{e^2 k_B T_n^*}{h} e^{\Delta^{\#} S^0/R}, \qquad (4.11)$$

where R is the gas constant and $\Delta^{\#}S^0$ is the standard entropy of activation (see, for example, ref. 40). For the temperature we apply the effective temperature given in eqn. (4.6). For one-photon absorptions T^*_n is typically 800–1000 K and the front factor in eqn. (4.11) becomes approximately 10^{14} s^{-1} which equals A when there is no structural order difference ($\Delta^{\#}S^0 = 0$). With an ordered transition state the number may be somewhat lower. For example, $\Delta^{\#}S^0 = -40$ J K^{-1} mol^{-1} yields A of the order of 10^{12} s^{-1}

Delayed photofragments are detected in ELISA with a detector which, unfortunately, does not provide any information about the masses of the detected particles. To get an idea of the possible fragments following excitation, low-energy collision-induced dissociation of both GFP and RFP chromophore ions was performed as described earlier. In the case of GFP^- the dominant dissociation process is loss of CH_3 (Scheme 1) by breaking of either a C–C or a C–N bond (see Fig. 2). The corresponding stretch frequency is of the order of 10^{13}–10^{14} s^{-1}. For GFP^+ the CID pattern was more complicated (Fig. 8) without a significant contribution corresponding to loss of a methyl group. The main peaks were at $m/z = 119$, 160, and 186. By analyzing these data it is evident that the CID may involve a rather complicated molecular rearrangement with a corresponding significant change of entropy.

The activation energy, E_a, is of crucial importance to the decay rate. To estimate it, we calculated the dissociation energies of the chromophore ions at the B3LYP/6-311++G(2d,p)//PM3 level of theory.[22] A low-energy dissociation channel involves the loss of the methyl group from the N atom (position 1 in the imidazolinone ring—see Fig. 2), *i.e.* one C–N bond is broken. Some results of our calculations are summarized in Tables 1 and 2. The energy required for this particular fragmentation channel is about 2.1 eV for the anions and about 3.4 eV for the cations of the present study.[42] Note that the three forms have basically the same activation energy for this fragmentation mode which is not the case for other modes of decay as seen from Table 2. The calculation supports the experimental findings presented earlier in this paper (*viz.* that fewer photons are needed to fragment the GFP-anion chromophore compared to the GFP-cation case). However, there are most likely other dissociation channels for the cations which have a lower activation energy than the calculated 3.4 eV. This would explain why loss of CH_3 in the CID spectrum is a very weak channel.

4.6 Analysis of experimental decay curves

Having established some idea of the magnitudes of the pre-exponential factor and the activation energy, and, moreover, knowing whether we deal with one, two, or three photon absorptions, we are in a position to calculate the yield of neutral fragments as a function of time after laser excitation with the use of eqns. (4.9) and (4.10). Values for A and E_a may be obtained from fits to experimental data. To get a reliable result A and E_a must remain approximately the same when considering data recorded at different wavelengths assuming that the dissociation channel is the same.

We consider first GFP anions. Good fits were indeed obtained with $A = 1.6 \times 10^{15}$ s^{-1} and $E_a = 1.82$ eV in the entire wavelength region around the absorption maximum, as seen in Fig. 4. In Fig. 13, $\ln(k)$ is plotted as a function of $1/k_B T^*$, which yields a straight line with the slope $-E_a$ and an intersection with the abscissa at $\ln(A)$. The decay rate k and T^* were extracted from the calculations [eqns. (3.5) and (3.6)], with values of E_a and A obtained from fits to the experimental data (Fig. 4). Here k is the rate for an ensemble of monoenergetic ions, *i.e.*, G being a delta function around $E = 0$. Note that T^* depends on the wavelength as well as the activation energy. From the data in Fig. 13 it is found that A is of the order of 10^{15} s^{-1} and E_a is about 1.8 eV. Both values are in quite good agreement with expectations based on the Gaussian calculation (Table I) and the fragmentation channel established by CID.

The situation is more complicated in the GFP cation case since both one and two-photon absorptions are involved, and close to the absorption maximum where two-photon absorption dominates, the decay is so fast that a fit to the yield of neutrals as a function of time is meaningless. However, at the low-wavelength side of the maximum (266 to 380 nm) the observed decay is dominated by one-photon absorption which results in a relatively slow decay (see also Fig. 5).

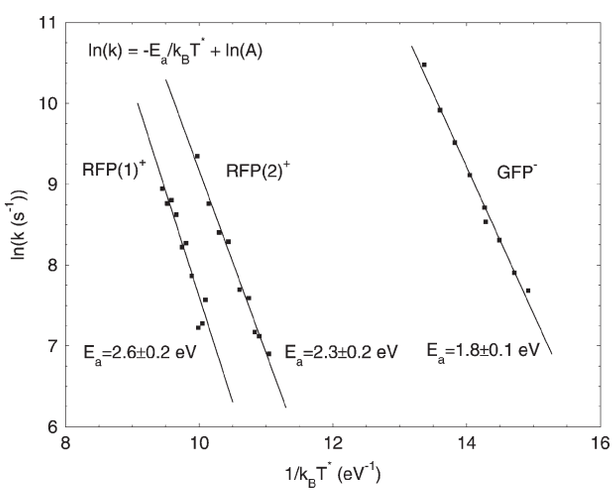

Fig. 13 The calculated $\ln(k)$ as a function of $1/k_B T^*$ obtained from individual fits (Eq. 9) to the data (see Figs. 3 and 5). The GFP anion was for $n = 1$ absorption, the RFP cations were for $n = 2$ absorption. Values of the pre-exponential factor are found in Table 3.

Since the decay is happening over a substantial time, there may be some competition by infrared radiative cooling which makes the decay appear faster than it would be without infrared emission. This may yield a slightly overestimated pre-exponential factor or underestimated activation energy. The effect may be more significant at longer wavelengths where the decay after one-photon absorption is slower. To determine A and E_a, data for $n = 2$ absorption at 430 nm and $n = 1$ absorption at 266 nm were fitted. Both sets of data could be accounted for with the values $A = 5 \times 10^{16}$ s^{-1} and $E_a = 3.0$ eV, as shown in Fig. 14. The high pre-exponential factor signifies simple cleavage and the obtained activation energy is in reasonable agreement with that calculated for methyl loss (Table 1). We do not see loss of methyl in the CID measurement with GFP^+ perhaps because fragmentation occurs by other channels of lower activation energy and pre-exponential factor before the temperature gets sufficiently high to cause methyl loss.

The GFP^+ data recorded at 355 nm appears to have two time components (see Fig. 5), which at first sight might be attributed to a one- and a two-photon absorption process. The power-dependence measurement, however, did not confirm that two different orders of absorptions were involved. The long-time component of about 9 ms and a quantum yield of about 0.50 is attributed to population trapping in a long-lived triplet state since no reasonable combination of A and E_a could account for this and the fast component at the same time. An alternative explanation could be that the ions occupy two different forms of the chromophore corresponding to two different sites of protonation. The shorter component may be due to a $n = 1$ statistical decay in the singlet manifold with an activation energy of 2.2–2.5 eV with a pre-exponential factor of 10^{15}–10^{17} s^{-1}. It does suggest that another dissociation channel is involved at this photon energy ($n = 1$, 3.5 eV) which has a lower activation energy than that involved at 430 nm ($n = 2$, 5.77 eV) and at 266 nm ($n = 1$, 4.66 eV).

We now turn to a discussion of the results obtained with the RFP chromophores. The power-dependence measurements discussed earlier revealed that the observed decays of the RFP model chromophores are due to absorption of two photons (for cations) and two and three photons (for anions). The data obtained with the smallest protonated form, $RFP(1)^+$, could be accounted for by a component with a lifetime between 0.5 ms and 3 ms varying with energy as $\exp(-E_{tot}(\text{eV})/0.35)$, where E_{tot} is the total internal energy ($2h\nu + E_0$). The remaining fast decay was simulated over the entire absorption profile (430–480 nm) by a statistical calculation with an activation energy of 2.6 ± 0.2 eV and a corresponding pre-exponential factor of the order of 10^{14}–10^{16} s^{-1}. $\ln(k)$ is plotted as a function of $1/k_B T^*$ in Fig. 13. The yield of fragments for the large protonated form, $RFP(2)^+$, could likewise be accounted for by a component with a ms-lifetime, also varying with energy as $\exp(-E_{tot}(\text{eV})/0.35)$. The data were corrected for this component and the remaining fast decay was simulated over the absorption profile (430–480 nm) by the statistical model yielding an activation energy of 2.3 ± 0.2 eV and a corresponding pre-exponential factor of the order of 10^{14} to 10^{15} s^{-1}. Again, $\ln(k)$ is plotted as a function of $1/k_B T^*$ in Fig. 13.

The two deprotonated chromophores $RFP(1)^-$ and $RFP(2)^-$ both exhibit a decay with three components. The longest component is attributed to one-photon absorption possibly with trapping in a triplet state and hence very slow dissociation. There are two possibilities for the origin of the two short components on the near ms and sub-ms time scales. They may be due to fragmentation in the singlet manifold after two and three $S_0 \rightarrow S_1$ excitations. Alternatively, fragmentation may occur after a photocycle involving the triplet state with two and three $S_0 \rightarrow S_1$ excitations followed by intersystem crossing into T_1. Dissociation will then be slower due to the (unknown) $T_1 - S_0$ electronic excitation energy which is not available for dissociation.

The ms time component is likely to be due to trapping in the T_1 state. At the maximum of absorption we obtain quantum yields which are of the order of 0.5–0.7 for all RFP chromophores, and the triplet lifetimes were 1 ms, 1.1 ms, 2.8 ms, and 3.5 ms for $RFP(1)^+$, $RFP(2)^+$, $RFP(1)^-$, and $RFP(2)^-$, respectively. It is the transition from the singlet excited state to the triplet state which is responsible for the blinking effect of fluorescent proteins and dark periods of ms duration have indeed been found for DsRed.[43] Moreover, a longer dark

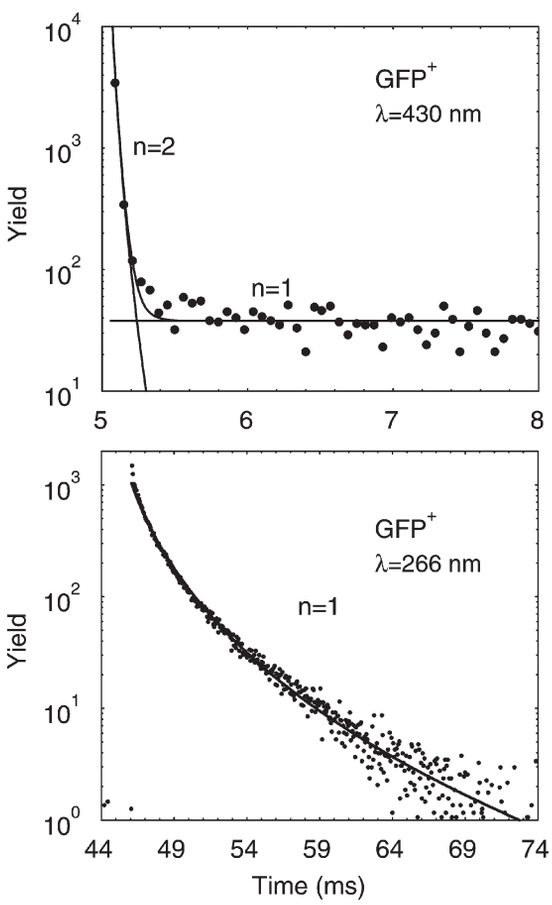

Fig. 14 Yield of neutral fragments as a function of time after laser excitation of GFP^+ at 430 nm and 266 nm. The solid lines are based on calculations with $E_a = 3.03$ eV and $A = 5 \times 10^{16}$ s^{-1}.

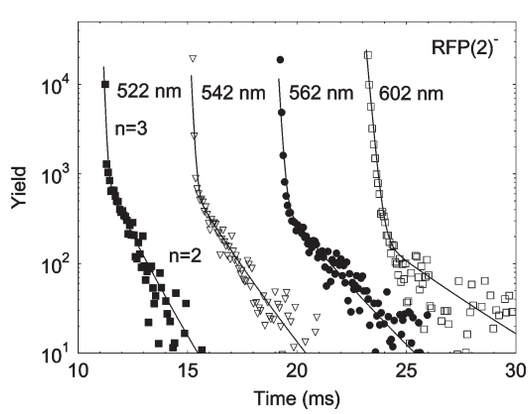

Fig. 15 Yield of neutral fragments from $RFP(2)^-$ as a function of the time recorded at four different wavelengths. The data have been separated in time for the purpose of better display. The curves are the calculated yield for $n = 2$ and 3 with $E_a = 1.12$ eV and $A = 10^8$ s^{-1}. A long-lived component has been subtracted.

Table 3 Summary of the results of the present study

Chromophore	GFP^-	GFP^+	GFP^+	$RFP(1)^-$	$RFP(1)^+$	$RFP(2)^-$	$RFP(2)^+$
E_a/eV	1.8 ± 0.1	2.2–2.5	3.0 ± 0.1	1.45 ± 0.1	2.6 ± 0.2	1.1 ± 0.1	2.3 ± 0.2
A/s^{-1}	$\sim 10^{15}$	10^{15}–10^{17}	10^{16}–10^{17}	$\sim 10^{9}$	10^{14}–10^{16}	$\sim 10^{8}$	10^{14}–10^{15}
λ/nm	440–510	355	430 (266)	470–570	430–480	500–600	430–480
n	1	1	2 (1)	2	2	2	2
E_{tot}/eV	2.8–3.2	3.8	5.0 (6.1)	4.7–5.7	5.6–6.2	4.5–5.4	5.6–6.2
T/K	950–1030	1130	1350 (1540)	1240–1400	1325–1425	1250–1410	1225–131

period of 6.3 ms was found for a GFP variant[43] in qualitative agreement with our results (9 ms at 355 nm for GFP^+).

Assuming that the $n = 2$ and $n = 3$ photocycle only involves the singlet states, we could at all wavelengths account for both the $n = 2$ and $n = 3$ components of the decay for $RFP(1)^-$ and $RFP(2)^-$ with the *same* set of values of E_a and A. Selected data and the calculations are shown in Fig. 15 for $RFP(2)^-$. The result is $E_a = 1.45$ eV and $A = 2 \times 10^9$ s^{-1} for $RFP(1)^-$ and is $E_a \sim 1.1$ eV and $A = 10^8$ s^{-1} for $RFP(2)^-$. The activation energy, as well as the pre-exponential factor, are significantly lower than the values obtained for the other chromophores in this study (see Table 3). The low pre-exponential factor signifies that a structured transition state is involved. From the CID spectra (Fig. 7) we know that several dissociation channels are open, and the decay may involve loss of $2CH_3$ (possibly ethane) and ring cyclization between the N-carrying CH_3 and the ethylenic side group. In the case of RFP(2) a six-membered ring is formed (see Scheme 2).

An important channel for the GFP chromophores is apparently the loss of methyl from nitrogen at position 1 and Gaussian calculations (Table 1) predict that the activation energy is almost identical for the chromophores of the present study. We find that the $n = 2$ time component of the $RFP(2)^-$ data (shown in Fig. 15) can be accounted for if E_a is of the order of 2.5 eV and $A \sim 10^{15}$ s^{-1} which could be realistic values for the methyl loss channel. However, the *same* set of values of E_a and A cannot reproduce the decays across the absorption profile and, moreover, the calculated $n = 3$ component with $E_a \sim 2.5$ eV and $A \sim 10^{15}$ s^{-1} is decaying much faster than the observation. It indicates that this dissociation channel is, indeed, slow (E_a high, A low) and hence cannot compete with other dissociation channels for $RFP(2)^-$. If the photocycle involves dissociation from the triplet state, the decay is slower due to a lower temperature of the chromophore (a consequence of the electronic energy stored in the triplet state). The triplet excitation energy is unknown and this prevents us from making calculations of the corresponding decay rates.

5 Conclusions

To summarize, the electrostatic storage ring ELISA was used to study photofragmentation of model chromophores of the fluorescent proteins GFP and RFP in the gas phase. The chromophores are heated up as a consequence of single and multiple absorptions and reach temperatures of about 1000–1500 K. Dissociation happens as a thermally activated process of the Arrhenius type. The decay rate of dissociation is on the ms-time scale and can be modeled in a calculation which takes into account the initial temperature of the chromophores. Based on the measured decay rate, fitted values of the activation energy, dft calculations, and collision-induced dissociation measurements, we conclude that loss of methyl is the dominating decay for the deprotonated GFP chromophore and for the protonated GFP chromophore at high temperature. At low temperature methyl loss is most likely not involved for GFP^+. Ring cleavage with lower activation energy may be an active channel. Other channels are most likely involved for the other chromophore ions. It is, in particular, noted that deprotonated RFP chromophores may decay through an ordered transition state. We can see an evidence for high quantum yields for trapping in long-lived (ms) triplet states.

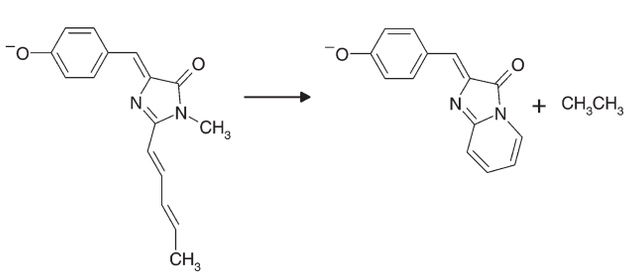

Scheme 2

Acknowledgements

We thank Steen Uttrup Pedersen and Peter Tonge providing some of the chromophore material used in this work. This work was supported by the Danish National Research Foundation through the Aarhus Center for Atomic Physics (ACAP). S.B. acknowledges the support by the European Community's Research Training Networks Program under contract HPRN-CT-2000-0142, ETR. SBN acknowledges the Danish Natural Science Research Council for a Steno grant.

References

1 R. W. Schoelein, L. A. Peteanu, R. A. Mathies and C. V. Shank, *Science (Washington, D. C.)*, 1991, **254**, 412–415.
2 L. Stryer, *J. Biol. Chem.*, 1991, **266**, 10 711–10 714.
3 R. Y. Tsien, *Annu. Rev. Biochem.*, 1998, **67**, 509–544.
4 A. B. Cubitt, R. Heim, S. R. Adams, A. E. Boyd, L. A. Gross and R. Y. Tsien, *Trends Biochem. Sci.*, 1995, **20**, 448–455.
5 D. C. Prasher, *Trends Genet.*, 1995, **11**, 320–323.
6 H.-H. Gerder and C. Kaether, *FEBS Lett.*, 1996, **389**, 44–47.
7 A. D. Kummer, J. Weihler, H. Rehaber, K. Kompa, B. Steipe and M. E. Michel-Beyerle, *J. Phys. Chem. B*, 2000, **104**, 4791.
8 H. Morise, O. Shimomura, F. H. Johnson and J. Winant, *J. Biochemistry*, 1974, **13**, 2656.
9 H. Niwa, S. Inouye, T. Hirano, T. Matsuno, S. Kojima, M. Ohashi and F. Tsuji, *Proc. Natl. Acad. Sci., U. S. A.*, 1996, **93**, 13 617–13 622.
10 C. Schweitzer and J. C. Scaiano, *Phys. Chem. Chem. Phys.*, 2003, **5**, 4911–4917.
11 S. B. Nielsen, A. Lapierre, J. U. Andersen, U. V. Pedersen, S. Tomita and L. H. Andersen, *Phys. Rev. Lett.*, 2001, **87**, 2281 021.
12 L. H. Andersen, A. Lapierre, S. B. Nielsen, I. B. Nielsen, S. U. Pedersen, U. V. Pedersen and S. Tomita, *Eur. Phys. J. D.*, 2002, **20**, 597–600.
13 S. Boyé, I. B. Nielsen, S. B. Nielsen, H. Krogh, A. Lapierre, H. B. Pedersen, S. U. Pedersen, U. V. Pedersen and L. H. Andersen, *J. Chem. Phys.*, 2003, **119**, 338–345.
14 S. Boyé, S. Brøndsted Nielsen, H. Krogh, I. B. Nielsen, U. V. Pedersen, A. F. Bell, X. He, P. J. Tonge and L. H. Andersen, *Phys. Chem. Chem. Phys.*, 2003, **5**, 3021–3026.
15 S. Boyé, H. Krogh, I. B. Nielsen, S. B. Nielsen, S. U. Pedersen, U. V. Pedersen, L. H. Andersen, A. F. Bell, X. He and P. J. Tonge, *Phys. Rev. Lett.*, 2003, **90**, 118 103-1.

16 S. P. Møller, *Nucl. Instrum. Methods Phys. Res., Sect. A*, 1997, **394**, 281–286.
17 J. U. Andersen, P. Hvelplund, S. B. Nielsen, S. Tomita, H. Wahlgreen, S. P. Møller, U. V. Pedersen, J. S. Forster and T. J. D. Jørgensen, *Rev. Sci. Instrum.*, 2002, **73**, 1284–1287.
18 It was experimentally verified that the absorption spectra did not change significantly with time after 10 ms of storage.
19 N. M. Webber, K. L. Litvinenko and S. R. Meech, *J. Phys. Chem. B*, 2001, **105**, 8036.
20 X. He, A. F. Bell and P. J. Tonge, *J. Phys. Chem. B*, 2002, **106**, 6056.
21 M. V. Matz, A. F. Frakov, Y. A. Labas, A. P. Savitsky, A. G. Zaraisky, M. L. Markelov and S. A. Lukyanov, *Nature Biotechnol.*, 1999, **16**, 969.
22 M. J. Frisch, G. W. Trucks, H. B. Schlegel, G. E. Scuseria, M. A. Robb, J. R. Cheeseman, V. G. Zakrzewski, J. A. Montgomery Jr., R. E. Stratmann, J. C. Burant, S. Dapprich, J. M. Millam, A. D. Daniels, K. N. Kudin, M. C. Strain, O. Farkas, J. Tomasi, V. Barone, M. Cossi, R. Cammi, B. Mennucci, C. Pomelli, C. Adamo, S. Clifford, J. Ochterski, G. A. Petersson, P. Y. Ayala, Q. Cui, K. Morokuma, D. K. Malick, A. D. Rabuck, K. Raghavachari, J. B. Foresman, J. Cioslowski, J. V. Ortiz, B. B. Stefanov, G. Liu, A. Liashenko, P. Piskorz, I. Komaromi, R. Gomperts, R. L. Martin, D. J. Fox, T. Keith, M. A. Al-Laham, C. Y. Peng, A. Nanayakkara, C. Gonzalez, M. Challacombe, P. M. W. Gill, B. G. Johnson, W. Chen, M. W. Wong, J. L. Andres, M. Head-Gordon, E. S. Replogle and J. A. Pople, GAUSSIAN98 (Revision A.9), Gaussian, Inc., Pittsburgh, PA, 1998.
23 Our calculations show that only *ca.* 10% of the vibrational modes of the chromophores studied here have an energy below 200 cm^{-1}.
24 R. González-Luque, M. Garavelli, F. Bernardi, M. Merchán, M. A. Robb and M. Olivucci, *Proc. Natl. Acad. Sci.*, 2000, **97**, 9379.
25 N. Ferré and M. Olivucci, *J. Am. Chem. Soc.*, 2003, **125**, 6868.
26 D. Mandal, T. Tahara, N. M. Webber and S. R. Meech, *Chem. Phys. Lett.*, 2002, **358**, 495.
27 M. J. Bearpark, F. Bernardi, S. Clifford, M. Olivucci, M. A. Robb, B. R. Smith and T. Vreven, *J. Am. Chem. Soc.*, 1996, **118**, 169.
28 W. Weber, V. Helms, J. A. McCammon and P. W. Langhoff, *Proc. Natl. Acad. Sci., U. S. A.*, 1999, **96**, 6177–6182.
29 J. El Yazal, F. G. Prendergast, D. Elliot Shaw and Y.-P. Pang, *J. Am. Chem. Soc.*, 2000, **122**, 11 411–11 415.
30 A. A. Voityuk, M.-E. Michel-Beyerle and N. Rösch, *Chem. Phys. Lett.*, 1997, **272**, 162–167.
31 A. A. Voityuk, M.-E. Michel-Beyerle and N. Rösch, *Chem. Phys. Lett.*, 1998, **231**, 13–25.
32 V. Helms, C. Winstead and P. W. Langhoff, *J. Mol. Struct.*, 2000, **506**, 179–189.
33 H. Tiefenthaler, *et al.*, *Helv. Chim. Acta*, 1967, **50**, 2244.
34 N. J. Turro, *Modern Molecular Photochemistry*, University Science Books, Sausalito, California, 1991.
35 G. N. Phillips Jr., *Curr. Opin. Struct. Biol.*, 1997, **7**, 821.
36 M. C. Chen, C. R. Lambert, J. D. Urgitis and M. Zimmer, *Chem. Phys.*, 2001, **270**, 157.
37 A. Toniolo, G. Granucci and T. J. Martínez, *J. Phys. Chem. A*, 2003, **107**, 3822.
38 This is not true when absorption from the triplet state is considered since the $T_1 \rightarrow T_n$ transition requires a preceeding $S_0 \rightarrow S_1$ transition.
39 J. U. Andersen, E. Bonderup and K. Hansen, *J. Chem. Phys*, 2001, **114**, 6518.
40 D. A. McQuarrie and J. D. Simon, *Physical Chemistry*, University Science Books, Sausalito, California, 1997.
41 T. Baer, W. L. Hase, *Unimolecular Reaction Dynamics*, Oxford University Press, Oxford, New York, 1996.
42 The detachment energy of the deprotonated GFP chromophore is calculated to be 2.86 eV, *i.e.*, higher than the energy required for dissociation.
43 M. Cotlet, J. Hofkens, F. Kohn, J. Michiels, G. Dirix, M. Van Guyse, J. Vanderleyden and F. C. De Schryver, *Chem. Phys. Lett.*, 2001, **336**, 415.